Supporting Information

Young and Panfilov 10.1073/pnas.1008837107

SI Text

SI Model. ***Basics of cardiac propagation.*** Synchronized contraction of the heart is initiated by propagating electrical waves of excitation. In normal conditions the excitation of the heart originates in the sinoatrial (SA) node (Fig. S1 and Fig. S2*A*), which is located in the right atrium. The SA node is a small strip of specialized muscle that is capable of self-excitation. The impulse that originates in the SA node travels outward in all directions and excites the two atria (Fig. S2*B*). The excitation is transmitted from atria to the ventricles of the heart at the atrioventricular (AV) node, which is located in the intraatrial wall between the atria and the ventricles. The propagation through the AV node is very slow, which results in a delay between the atrial excitation and the ventricular excitation and causes the atria to contract earlier than the ventricles. The impulse spreads rapidly from the AV node through a specialized conducting system to the muscle fibers of the ventricles (Fig. S2*C*). The conducting system is formed by the bundle of His, its branches and the Purkinje fibers, and transmits impulses to the endocardial surface of the left and right ventricle. Following propagation through the Purkinje fibers the excitation enters the ventricular tissue and activates the ventricles of the heart, causing ventricular contraction (Fig. S2*D*).

Propagation of excitation in cardiac tissue is anisotropic; the myocardium is arranged into muscle fibers, as shown in Fig. 1 of the main text, and the propagation along cardiac fibers is 2–3 times faster than across them. Studies of cardiac anatomy (1) have identified that speeds may also vary transverse to the fibers; the fibers in the heart are locally organized into sheets, and there is higher connectivity inside a sheet than transverse to it. This electrophysiological anisotropy is the basis for our introduction of the *el*-metric.

Details of ionic model simulations.

1. Methods.

Cardiac tissue was modeled by the following system of parabolic partial differential equations (2–4):

$$\frac{\partial V}{\partial t} = -\frac{I_{\text{ion}}}{C_m} + \text{div}(i). \qquad \textbf{[S1]}$$

$$i_x = (D_1 \cos^2\theta + D_2 \sin^2\theta)\frac{\partial V}{\partial x} + (D_1 - D_2)\sin\theta\cos\theta\frac{\partial V}{\partial y}; \qquad \textbf{[S2]}$$

$$i_y = (D_2 \cos^2\theta + D_1 \sin^2\theta)\frac{\partial V}{\partial y} + (D_1 - D_2)\sin\theta\cos\theta\frac{\partial V}{\partial x}; \qquad \textbf{[S3]}$$

$$i_z = D_3\frac{\partial V}{\partial z}; \qquad \textbf{[S4]}$$

where (x,y,z) denotes the Cartesian coordinate system, with the slab parallel to the xy-plane. The term θ is the angle between the fiber direction and the (fixed) x axis, and depends on the z variable only (fibers are assumed to lie in parallel planes), and D_1, D_2, D_3 measure conductance longitudinally along fibers, orthogonal to the sheets, and perpendicular to the slab respectively. $C_m = 1\ \mu\text{F/cm}^2$ represents the membrane capacitance and I_{ion} is the sum of all transmembrane ionic currents.

The system **[S1–S4]**, along with additional expressions for I_{ion}, describes action potential dynamics in continuous cardiac tissue.

For numerical simulations we use a discretization (2, 5) with equal space steps h in the x, y and z direction and evaluate needed derivatives using the approximations

$$\begin{aligned}
\partial^2 V/\partial x^2 &= (V(x+h,y,z) + V(x-h,y,z) - 2.*V(x,y,z))/h^2\\
\partial^2 V/\partial y^2 &= (V(x,y+h,z) + V(x,y-h,z) - 2.*V(x,y,z))/h^2\\
\partial^2 V/\partial z^2 &= (V(x,y,z+h) + V(x,y,z-h) - 2.*V(x,y,z))/h^2\\
\partial^2 V/\partial x\partial y &= (V(x+h,y+h,z) + V(x-h,y-h,z)\\
&\quad - V(x-h,y+h,z) - V(x+h,y-h,z))/4h^2
\end{aligned}$$

Here V is the transmembrane potential and t is time.

We use the Luo-Rudy phase 1 model (LR1) (6) for the calculation of the total current: $I_{\text{ion}} = I_{Na} + I_{si} + I_K + I_{K1} + I_{Kp} + I_b$, where $I_{Na} = G_{Na}m^3hj(V - E_{Na})$ is the fast Na^+ current, $I_{Si} = G_{Si}df(V - E_{Si})$ is the slow inward Ca^{2+} current, $I_k = G_k x x_1(V - E_k)$ is the slow outward K^+ current, $I_{K1} = G_{K1}K1_\infty(V - E_{K1})$ is the time-independent K^+ current, $I_{Kp} = G_{Kp}K_p(V - E_{Kp})$ is the plateau K^+ current, and $I_b = G_b(V - E_b)$ is the background current. The variables m, h, j, d, f and x are gating variables, which dynamics can be modeled by

$$\frac{dy}{dt} = (y_\infty - y)/\tau_y, \qquad \textbf{[S5]}$$

where y represents any of the gating variables. We use standard parameters from (3, 4, 6) with $G_{Na} = 16.0\ \text{mS/cm}^2$. For more details of the model see ref. 6.

We integrated Eq. **S1** by the Euler method with time step $\Delta t = 0.003$ ms and used finite differences with a space step of $\Delta x = 50\ \mu$m to calculate the Laplacian. We used diffusion coefficients in the ratio $D_1{:}D_2{:}D_3 = 1{:}0.0625{:}0.25$, with $D_1 = 0.001\ \text{cm}^2/\text{ms}$. We simulated a one-dimensional cable to find the speed of propagation in different directions, obtaining velocities of 0.58 m/s (in the fiber direction), 0.29 m/s (in the sheet direction), and 0.13 m/s in the normal direction.

Simulations were also performed using the eikonal model described in the main text.

For most of the 3D computations we used a $600 \times 600 \times 90$ grid for the ionic model and a $400 \times 400 \times 60$ grid for the eikonal model. Thus, the space step in the eikonal model was 50% larger than in the ionic simulations.

2. Results.

2.1. Standard tests.

We performed the ionic simulations with a space step of $\Delta x = 50\ \mu$, which is about 3–5 times smaller than the accepted value of the spacestep used to study 3D wave propagation in ionic models (7, 8). One difficulty was that the orientation of the fibers with respect to the grid seems to have an effect on propagation speed; we also simulated individual layers (i.e., $600 \times 600 \times 1$ slabs with parallel fibers) and obtained fiber velocities ranging from 0.58 m/s (when fibers were parallel to the x or y axis) to 0.55 m/s (when fibers were at a 45° angle to the axes) and normal velocities ranging from 0.13 m/s (when fibers were parallel to the x or y axis) to 0.18 m/s (when fibers were at a 45° angle to the axes). Thus, even with such a small space step, velocities varied substantially, and the model did not reproduce the expected 4:1 anisotropy. In contrast, a similar test with the eikonal model showed some grid effects, but at a much smaller level, with fiber velocities ranging from 0.55 m/s (fibers parallel to an axis) to 0.52 m/s (fibers at 45°) and normal velocities of 0.14 m/s regardless of direction.

2.2. Twisted slab.

We simulated a 30 mm × 30 mm × 4.5 mm twisted slab with 180° fiber rotation using both the ionic and the eikonal models.

Due to the variation in velocities mentioned above and the fact that the ionic model exhibits a slight delay between the stimulus and the first activation, we used a linear regression to fit the arrival times in the eikonal model to the arrival times in the ionic model; the velocities in the eikonal model after fitting were $v_f = 0.55$ m/s in the fiber direction, $v_s = v_f/2$ in the sheet direction, and $v_n = v_f/4$ in the normal direction.

Fig. S3 shows isochrones calculated using each model; the upper panels depict the ionic model and the lower panels depict the eikonal model, in 4 slices representing $z = 0$, 0.15, 0.3, 0.45 cm. We see good correspondence in all sections, though one can see that the velocity normal to the fibers seems slightly faster in the ionic model; the closely spaced contours on the left and right of the activation site (the center of the leftmost plot) are spaced a little more tightly in the eikonal model. We attribute this partly to the effect of grid direction mentioned in the previous subsection.

Despite this, the differences between the two simulations are slight. Fig. S4 shows a histogram of the absolute error between the two simulations; the difference in activation time between the two models is <1 ms in almost 95% of cases. We thus conclude that the eikonal model used in our simulations, even on a grid with larger space step, provides an accurate description of wave propagation in anisotropic heart tissue, possibly more accurate than the ionic model in some cases.

1. LeGrice IJ, et al. (1995) Laminar structure of the heart. II. Mathematical model. *Am J Physiol* 269:H571–H582.
2. Panfilov AV, Keener JP (1995) Reentry in three-dimensional myocardium with rotational anisotropy. *Physica D* 84545–552.
3. Garfinkel A, Qu Z (2000) Nonlinear dynamics of excitation and propagation in cardiac tissue. *Cardiac Electrophysiology. From Cell to Bedside*, 3rd edition, edited by DP Zipes, J Jalife (Saunders, Philadelphia), pp. 315–320.
4. Ten Tusscher KHWJ, Panfilov AV (2003) Reentry in heterogeneous cardiac tissue described by the Luo–Rudy ventricular action potential model. *Am J Physiol-Heart C* 284:H542–H548.
5. Fenton F, Karma A (1998) Vortex dynamics in three-dimensional continuous myocardium with fiber rotation: filament instability and fibrillation. *Chaos* 8:20–47.
6. Luo C, Rudy Y (1991) A model of the ventricular cardiac action potential. Depolarization, repolarization, and their interaction. *Circ Res* 68:1501–1526.
7. Garfinkel A, et al. (2000) Preventing ventricular fibrillation by flattening cardiac restitution. *Proc Natl Acad Sci USA* 97:6061–6066.
8. Xie F, et al. (2004) A simulation study of the effects of cardiac anatomy in ventricular fibrillation. *J Clin Invest* 113:686–693.

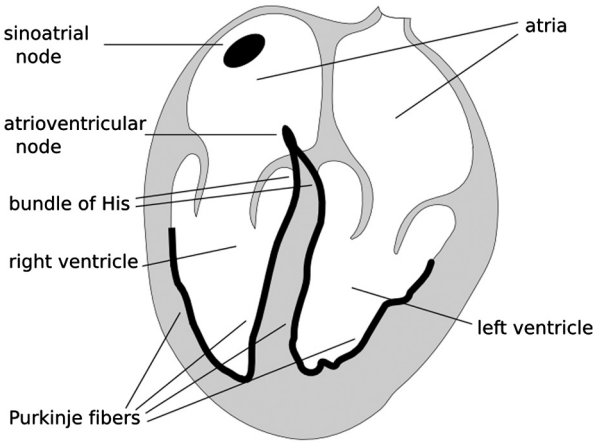

Fig. S1. Schematic cross section of the heart with parts of the conduction system labeled. Based on an illustration by Patrick J. Lynch, illustrator; C. Carl Jaffe, MD, cardiologist, released under a CC-by license.

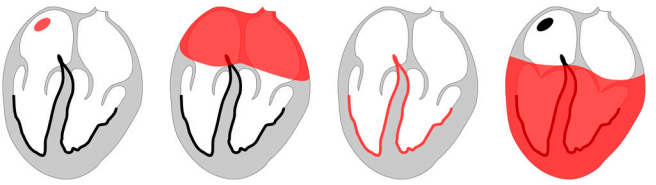

Fig. S2. Schematic of the progression of activation through the heart. In the first and second images, a wave of activation originates at the SA node and progresses through the atria. In the third and fourth, the wave is transmitted from the atria to the ventricles through the AV node, the bundle of His, and the Purkinje fibers. Based on an illustration by Patrick J. Lynch, illustrator; C. Carl Jaffe, MD, cardiologist, released under a CC-by license.

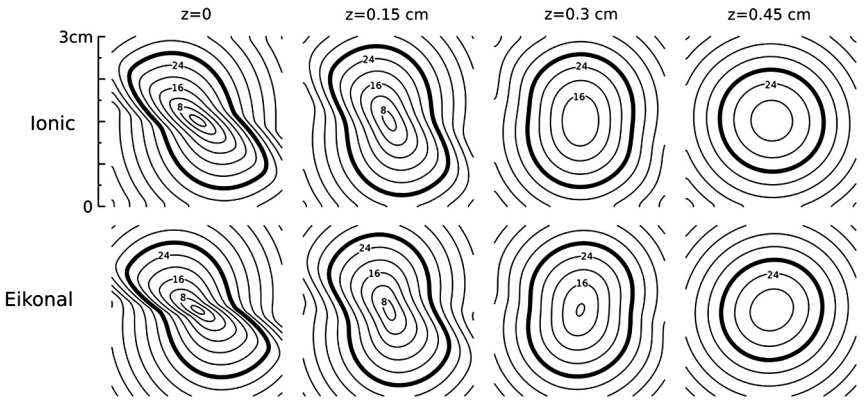

Fig. S3. Isochrones for activation times in the ionic and eikonal models. Isochrones are spaced 4 ms apart, and the $t = 28$ ms isochrone is highlighted by a thick line. The stimulus occurred at the top of the slab, that is, the center of the $z = 0$ plane.

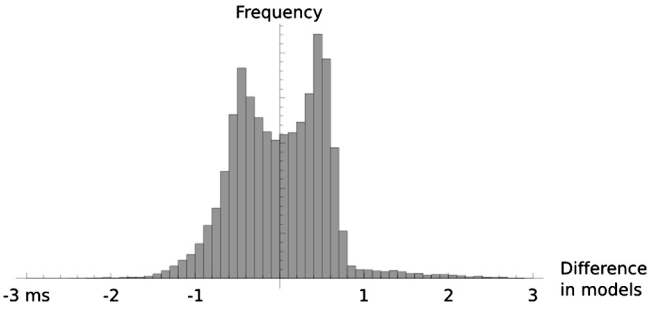

Fig. S4. A histogram of the difference in activation time between the two models. A positive difference means that the activation time for a point is earlier in the eikonal model; a negative difference indicates that the point was activated faster in the ionic model; zero difference means that the activation times in the two models are equal. The histogram was calculated based on $3 \cdot 10^4$ samples from the slab.

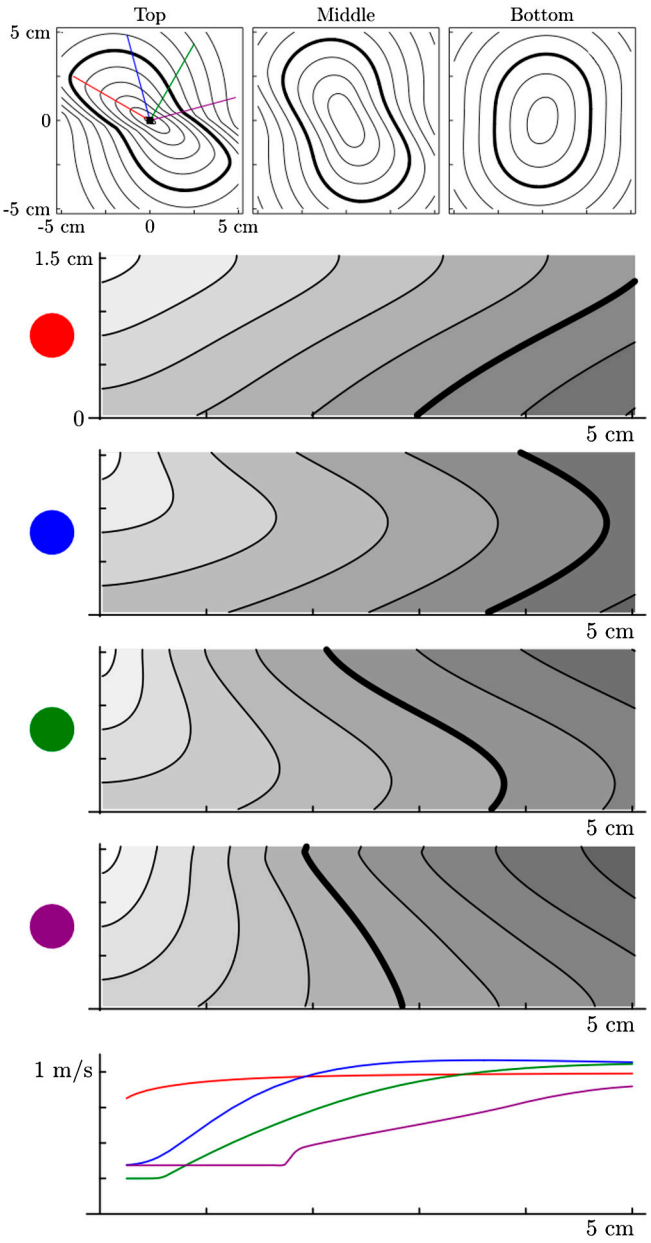

Fig. S5. Isochrones and transverse slices in a slab with 120° fiber rotation. Other parameters are as in Figs. 2 and 3 of the main text.

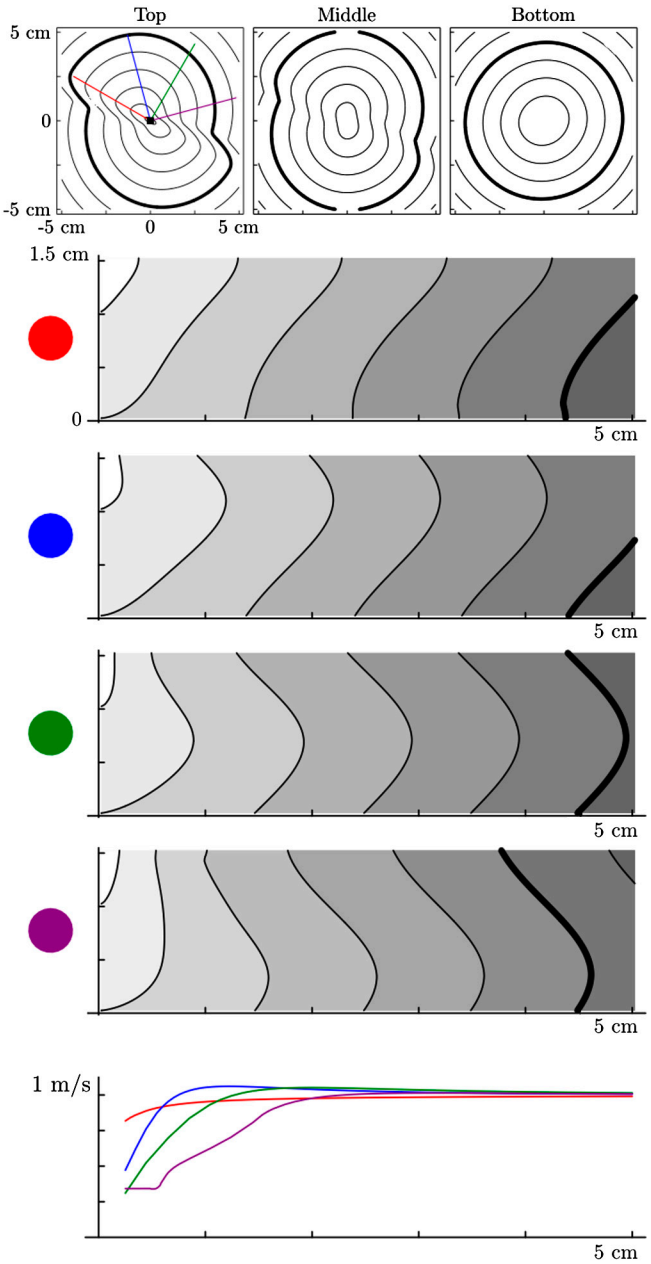

Fig. S6. Isochrones and transverse slices in a slab with $v_f = 1$ m/s, $v_s = 1$ m/s, $v_n = .25$ m/s. Other parameters are as in Figs. 2 and 3 of the main text.

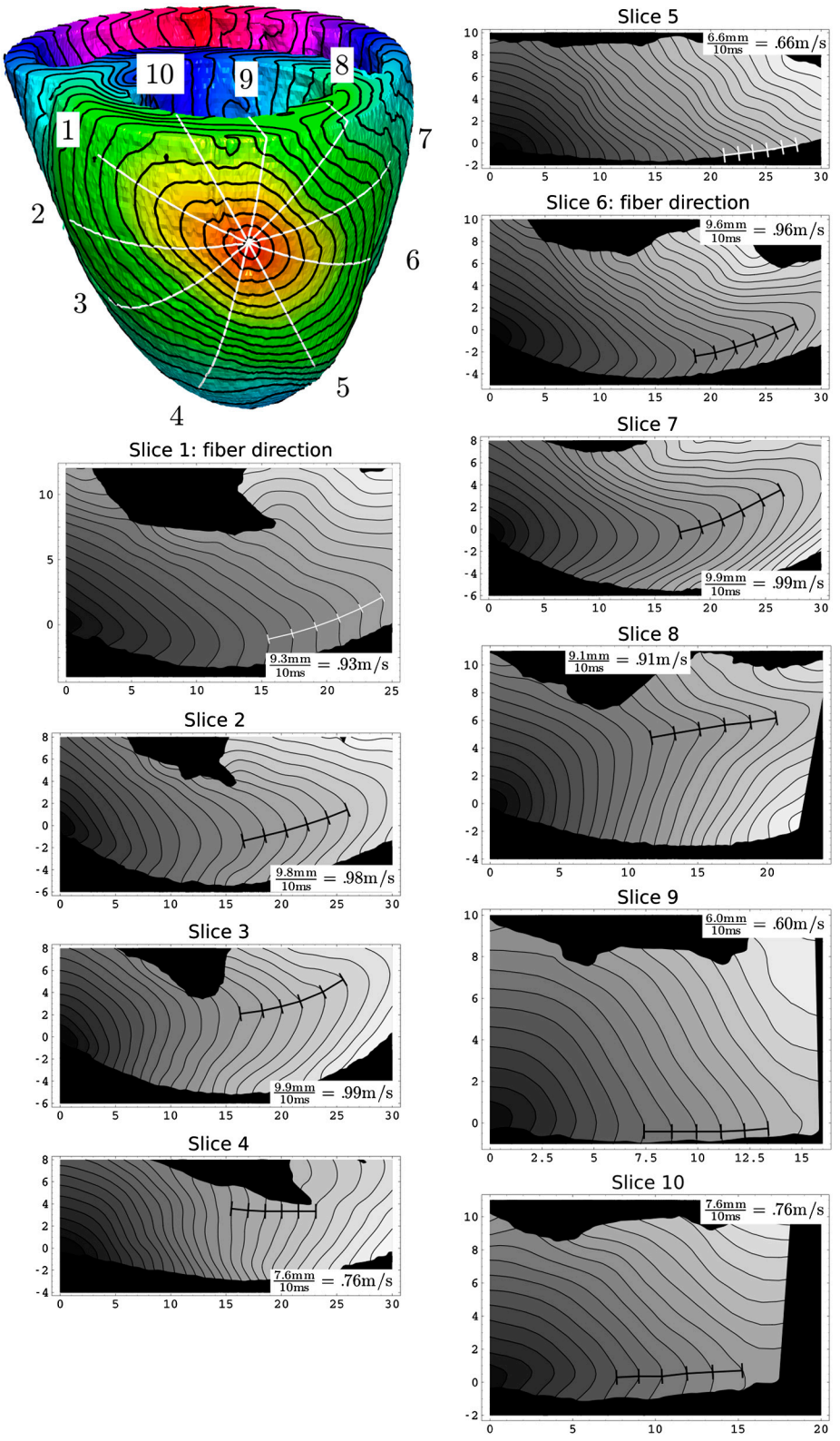

Fig. S7. Isochrones and transverse slices in the model of the ventricles; this figure extends Fig. 4 *A–D* in the main text.